Initial Spectral Polarimetry of Geosynchronous Satellites

David M. Strong
Strong EO Imaging, Inc.
Charles J. Wetterer
KBR
Timothy W. Giblin
i2 Strategic Services LLC
Cadet Matthew S. Fitzgerald, Francis K. Chun
Department of Physics and Meteorology, USAF Academy

ABSTRACT

The United States Air Force Academy (USAFA) has developed techniques to characterize and identify satellites since 2014 using a 16-inch telescope (USAFA-16) on campus as well as off-campus telescopes which comprise the Falcon Telescope Network (FTN). As part of this effort, USAFA has developed calibration techniques to enable identification of geosynchronous satellites through the polarization of satellites. USAFA recently acquired a 1-meter telescope (USAFA-1m) that has not yet been calibrated for polarization measurements. In this paper, we report on the effort to calibrate the USAFA-1m for polarimetry. For polarization calibrations we generate a transformation matrix to account for polarization effects of the optical system. Once calibrated, the USAFA-1m telescope will be capable of satellite characterization akin to that of the FTN.

1. INTRODUCTION

The United States Air Force Academy (USAFA) has a new 1-meter telescope (USAFA-1m) on its campus that is used for cadet education and research in space situational awareness (SSA) and astronomy. This new telescope complements a smaller 16-inch telescope (USAFA-16), also located on the USAFA campus, as well as USAFA's off-campus world-wide telescope network called the Falcon Telescope Network (FTN) [1]. These small telescopes (USAFA-16 and FTN) have been used to develop techniques to extract characteristics and features of artificial satellites solely from its unresolved signature using a variety of filters such as multi-spectral broadband color filters, transmission gratings, and linear polarizers [2-5]. The USAFA-1m telescope has similar filters, which we are starting to calibrate. This paper will present initial results of polarized spectra of geostationary (GEO) satellites using the polarization filters and transmission gratings. We first present specifications of the USAFA-1m telescope and imaging system, followed by the calibration process we used for the polarizers. The calibration of the transmission gratings is addressed in another paper associated with the 2023 AMOS Conference [6]. We end with initial measurements of polarized spectra of DirecTV-10, -12, and -15.

2. TELESCOPE SYSTEM

The USAFA-1m telescope is an Astro Systeme Austria, Ritchey-Chrétien design with an effective system f-number of f/6 (see Figure 1). The camera is a large-format Spectral Instruments CCD camera with a 16-sector focal plane of 9216 × 9232 pixels resulting in a plate scale of 0.34 arcseconds per pixel (see Figure 2). The field-of-view of the system is 52 × 52 arcminutes. Below is a list of characteristics and specifications of the telescope system. Additionally, two filter wheels in series are employed enabling the possibility of combined observations (e.g. polarization combined with a diffraction grating).

- 1-meter-diameter primary mirror (M1)
- System f/6
- Fork equatorial mount
- 6°/sec slew rate
- 9216 × 9232 pixel CCD camera with a pixel pitch of 10 mm
- Plate scale of 0.34 arcsec/pixel
- -100° C operating temperature
- Dual 8 square slot filter wheels
- Multi-spectral, broadband color filters: U, B, V, R, I (Kron-Cousins)
- Transmission gratings: 720 lines/mm, 200 lines/mm

- Polarizers (linear): 0°, 45°, 90°, 135° (relative to focal plane)

Fig. 1 Picture of the 1-meter telescope at the United States Air Force Academy.

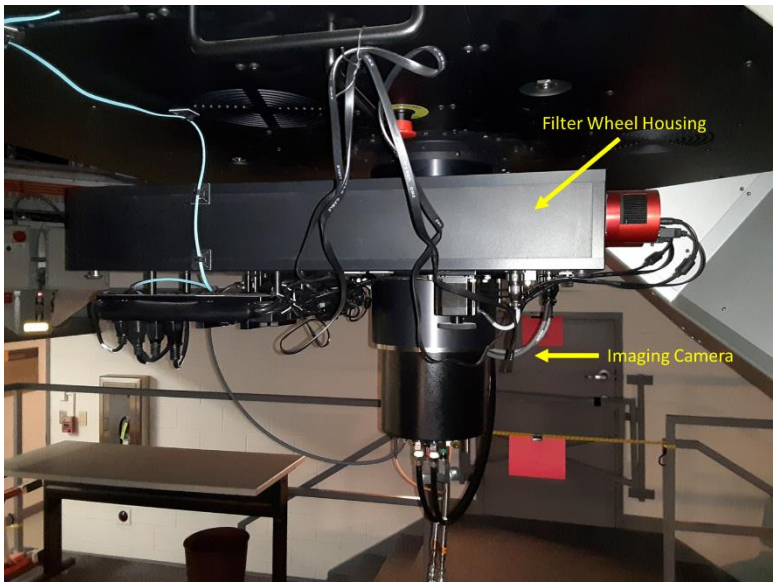

Fig. 2 Picture of the camera and filter wheel system.

Example images of the USAFA-1m camera are shown in Figure 3 to include (a) bias, (b) dark, (c) flat, and (d) raw science images. The bias image is by definition a zero-second exposure image and captures the noise due to the readout electronics of the camera's focal plane. The dark image on the other hand, captures the thermal noise of the focal plane with the camera shutter closed, and depends on exposure time and operating temperature of the camera. The filter-dependent flat describes the non-uniform response across the focal plane as well as any dust specks and other particulates on the optical surfaces between the primary mirror and the camera's focal plane. In Figure 3, both the dark and raw science images were taken with a 30-second exposure, while the flat and raw science images were taken using the R filter. The 16 sectors are clearly evident in all four types of images.

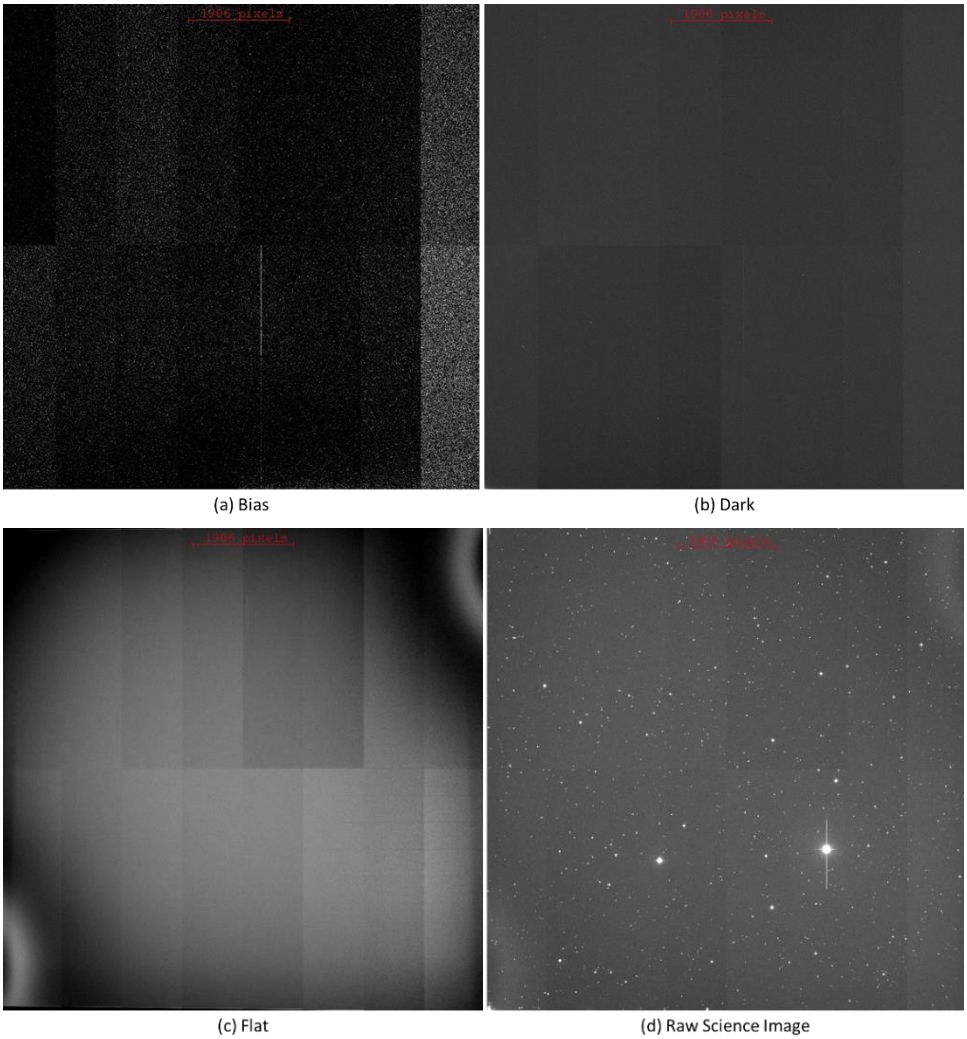

Fig. 3 Example of (a) bias, (b) dark, (c) flat, and (d) raw science images.

3. CALIBRATION OF POLARIZATION FILTERS

Polarization calibration of the USAFA-1m telescope is accomplished by taking sets of polarization images, one image for each polarization filter orientation. Figure 4 shows a single set of images taken of the Landolt Star Field SA26.

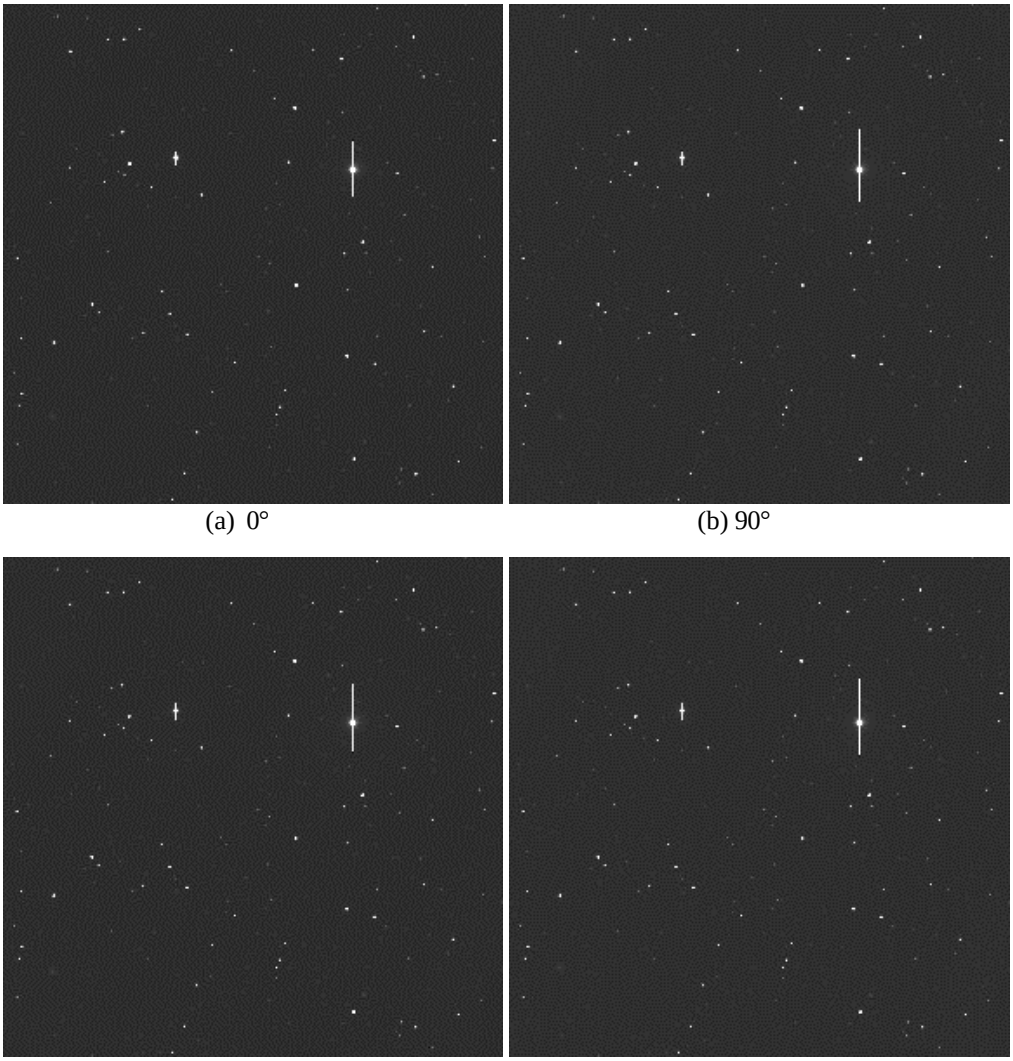

(a) 0° (b) 90°

(c) 45° (d) 135°

Fig 4. A set of polarization images: (a) 0°, (b) 90°, (c) 45°, and (d) 135°.

The counts for each star in each image are then extracted using Source Extractor. Then astrometry.net is used to solve for the right ascension (RA) and declination (DEC) for the image and the associated stars. Using the RA/DEC coordinates for the stars, the associated GAIA DR2 catalog value is found. The visible magnitudes (VM) from the GAIA catalog, along with the calculated instrument magnitude (IM) from the extracted counts, are used to calculate a pseudo zero point for the telescope with the specified filter.

$$VM = Gmag + 0.0176 + 0.00686*(G_{BP}-G_{RP}) + 0.1732*(G_{BP}-G_{RP})^2 \text{ [7]} \quad (1)$$

$$IM = -2.5 * \log10(Counts / Int\_Time) \quad (2)$$

$$ZP = VM - IM \quad (3)$$

The G magnitude has a broad pass band center in the green part of the spectrum, see Figure 5. The G_{BP} covers the blue side of the spectrum and the G_{RP} covers the red side. The visual magnitude calculation above takes into account the three measured bands. The counts are calculated by Source Extractor using a psf fitting function [8], and then divided by the integration time for the observation to calculate the instrument magnitude (Mag_Auto) in the table using Eq. 2. The pseudo zero-point (ZP) is then calculated using Eq. 3 and is considered a pseudo ZP because other

errors such as camera quantum efficiency, atmospheric extinction, etc. are not considered. A case for correcting for atmospheric extinction will be addressed later.

Table 1 shows example data extracted from SA26 using Source Extractor and the GAIA DR2 dataset. Each row contains the data for one star extracted from each image processed. There are many more columns in the output spreadsheet, but the table shows the relevant data for this study. The right ascension (RA) and declination (DEC) of the star are used to find the associated star in the DR2 catalog and extract the catalog magnitudes.

Table 1. Date 2023-02-11T05:39:15.235, ExpTime 20s, Filter P0 from SA26

RA	DEC	G_mag	BP_mag	RP_mag	Mag_Auto	Counts	Pseudo ZP
100.91	44.41972	8.368156	8.663708	7.959335	-18.8478	34603660	24.26622
100.91	44.41963	8.368156	8.663708	7.959335	-18.8119	33479206	24.23035
100.91	44.42073	8.368156	8.663708	7.959335	-18.8513	34714150	24.26968
100.91	44.42075	8.368156	8.663708	7.959335	-18.8585	34947104	24.27694
100.91	44.42071	8.368156	8.663708	7.959335	-18.883	35744772	24.30144

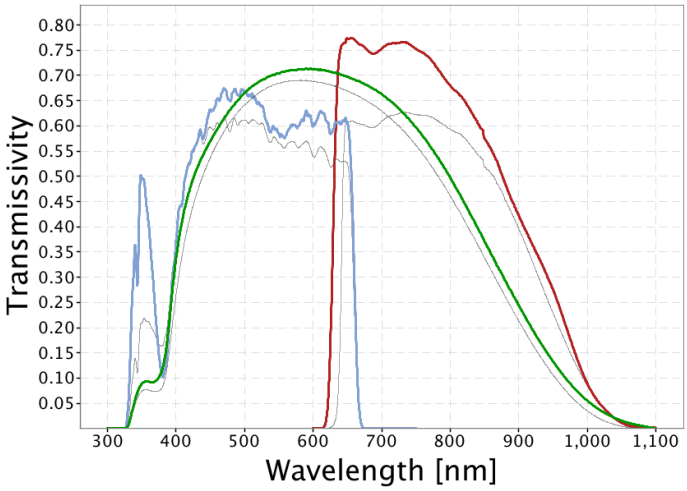

Fig. 5. GAIA DR2 passbands for G, G_{BP} and G_{RP} (green: G; blue: G_{BP}; red: G_{RP})
(from: https://www.cosmos.esa.int/web/gaia/iow_20180316)

4. POLARIZATION CALIBRATION METHODOLOGY

The next step was to extract the data for well-known calibration stars for each filter to determine any difference between them. Landolt star field SA26 was imaged on 10 February 2023. Ten observations were made with each polarization filter and the average of the pseudo ZP for 8 calibration stars within the field are shown in Table 2.

Table 2. Pseudo ZP Data from Cal Stars in SA26 without Noise Reduction

Cal Star	P00	P45	P90	P135
85	24.27	24.90	24.27	24.27
91	24.49	24.94	24.48	24.49
94	24.45	24.50	24.44	24.43
95a	24.58	24.45	24.57	24.55
95b	24.39	24.58	24.41	24.48
96	24.59	24.30	24.54	24.59
107	24.93	24.45	24.92	24.93
109	24.89	24.49	24.89	24.91
Mean	24.57	24.57	24.56	24.58
Std Dev	0.23	0.23	0.23	0.23

The data shows measurements across the filters are consistent with no noticeable differences. The data in Table 2 was extracted without the benefit of any noise reduction of the observations. The resulting means and standard deviations for each of the filters show no differences with any statistical significance.

In order to make a more accurate comparison, the images were noise-reduced using the appropriate bias, dark, and flat images taken using the telescope. The data in Table 3 was extracted using the noise reduced images. The mean ZP decreased by approximately 0.2 magnitudes with very little change in the standard deviation.

Table 3. Pseudo ZP Data from Cal Stars in SA26 with Noise Reduction

Cal Star	P00	P45	P90	P135
85	24.08	24.07	24.07	24.08
91	24.27	24.27	24.26	24.26
94	24.29	24.28	24.27	24.27
95a	24.37	24.37	24.35	24.35
95b	24.22	24.20	24.19	24.20
96	24.26	24.24	24.22	24.25
107	24.79	24.79	24.77	24.79
109	24.69	24.67	24.67	24.69
Mean	24.37	24.36	24.35	24.36
Std Dev	0.24	0.24	0.24	0.25

The resulting ZP means for all four filters are very similar and well within the standard deviation of each filter. So again, there is no statistical difference between the four polarization filters. If there were differences, the following calibration method would be used to calibrate future observations. Using the noise reduced ZP means from Table 3, the values in Table 4 are calculated.

Table 4. Calibration Matrix Development Values

	Mean ZP	IM Assuming 10th Mag	Exp Counts	Norm	Inverse
P0	24.37049	-14.3705	560009	1.010018	0.990081
P45	24.36076	-14.3608	555012	1.001005	0.998996
P90	24.34703	-14.347	548039	0.988429	1.011706
P135	24.36026	-14.3603	554759	1.000548	0.999452

Using the mean ZP for each filter, an instrument magnitude (IM) is calculated assuming a 10th magnitude star. This value is then used to generate an expected count for that IM using the inverse of Eq. 2 above. This is required to move the calibration from a magnitude scale to the observation count domain. The counts are normalized using the average of the expected counts. This is based on the expectation that the stars used are not polarized, which is the case for the calibration stars used.

This method follows from the linear algebra for the domain as follows:

$$AX = Y, \tag{4}$$

where

$$A = \begin{bmatrix} a_{11} & a_{12} & a_{13} & a_{14} \\ a_{21} & a_{22} & a_{23} & a_{24} \\ a_{31} & a_{32} & a_{33} & a_{34} \\ a_{41} & a_{42} & a_{43} & a_{44} \end{bmatrix}, X = \begin{bmatrix} I_{P0} \\ I_{P45} \\ I_{P90} \\ I_{P135} \end{bmatrix}, Y = \begin{bmatrix} I'_{P0} \\ I'_{P45} \\ I'_{90} \\ I'_{135} \end{bmatrix} \tag{5}$$

A is the calibration matrix, X are the measured intensities, and Y are the calibrated intensities where $I'_{P0} = I'_{P45} = I'_{P90} = I'_{P135} = (I_{P0} + I_{P45} + I_{P90} + I_{P135})/4 = I'$. There are many solutions to A, but the simplest solution is to use the expected values from Table 4 and plug in the values for the inverses along the diagonal for A resulting in

$$A = \begin{bmatrix} \frac{I'}{I_{P0}} & 0 & 0 & 0 \\ 0 & \frac{I'}{I_{P45}} & 0 & 0 \\ 0 & 0 & \frac{I'}{I_{P90}} & 0 \\ 0 & 0 & 0 & \frac{I'}{I_{P135}} \end{bmatrix} = \begin{bmatrix} 0.990081 & 0 & 0 & 0 \\ 0 & 0.998996 & 0 & 0 \\ 0 & 0 & 1.011706 & 0 \\ 0 & 0 & 0 & 0.999452 \end{bmatrix} \tag{6}$$

Using this result, the calibration matrix would be used to convert the raw counts from future observations into corrected counts:

$$\underbrace{\begin{bmatrix} I'_{P0} \\ I'_{P45} \\ I'_{90} \\ I'_{135} \end{bmatrix}}_{Corrected} = \underbrace{\begin{bmatrix} 0.990081 & 0 & 0 & 0 \\ 0 & 0.998996 & 0 & 0 \\ 0 & 0 & 1.011706 & 0 \\ 0 & 0 & 0 & 0.999452 \end{bmatrix}}_{Calibration\ Matrix} \underbrace{\begin{bmatrix} I_{P0} \\ I_{P45} \\ I_{P90} \\ I_{P135} \end{bmatrix}}_{Raw} \tag{7}$$

Once the observations are corrected for any systemic errors, the Stokes parameters (S0, S1, S2) are calculated, which are then used to determine the Degree-of-Linear-Polarization (DOLP) and the Angle-of-Linear-Polarization (AOLP). However, as seen in Table 2 and Table 3, all four polarization filters (P0, P45, P90, P135) essentially measure the same ZP within the uncertainties regardless of whether noise (e.g., bias, darks) is accounted for or not. Additionally, since we are more concerned with relative polarization instead of absolute polarization, we can simply process the polarization images as is without any correction.

5. EFFECTS OF NOISE ON THE POLARIZATION ZERO POINT

The following data shows the results of using a larger number of stars in the development of an automated pseudo ZP calculation and will work for any filter. Without the restriction of well-known calibration stars, the constraint

can be relaxed and all the stars within a magnitude range can be used because of the accuracy of the GAIA DR2 catalog. This accuracy is down the milli-mag range for the stars that can be observed by a 1-meter telescope. Tables 5 and 6 show the automated extraction of star data based on the GAIA DR2 magnitude data.

Table 5 – Polarization Zero Point without Noise Reduction

	Mag Range	**"11-14"**	**"12-14"**	**"12-13"**	**"13-14"**
P0	Ave ZP	24.95	24.94	24.97	24.92
	STD	0.33	0.32	0.33	0.32
P45	Ave ZP	25.00	25.00	25.05	24.97
	STD	0.36	0.33	0.18	0.39
P90	Ave ZP	24.96	24.96	24.98	24.95
	STD	0.40	0.38	0.36	0.39
P135	Ave ZP	24.97	24.97	24.99	24.95
	STD	0.36	0.36	0.31	0.38
	# of Stars	18,299	15,655	5,857	9,798

Table 5 shows the extracted pseudo ZP for several different GAIA G magnitude ranges. With the stars associated to a catalog value, the ZP is calculated, as above, for all stars in the ranges shown. For the “11-14” magnitude range, there are 18,299 stars extracted from the 40 images taken of the SA26 star field alone. The average ZP is shown for those stars along with the associated standard deviation. For the “12-14” magnitude range, 15,655 stars were used. For the “12-13” magnitude range, 5,857 stars were used. For the “13-14” magnitude range, 9798 stars were used. For the raw images, the ZP calculations and the standard deviations are consistent across the magnitude ranges. So, even without noise reduction, the results from the automated extraction still indicate no statistical difference across the four filters.

Table 6 - Polarization Zero Point with Noise Reduction

	Mag Range	**"11-14"**	**"12-14"**	**"12-13"**	**"13-14"**
P0	Ave ZP	24.79	24.78	24.77	24.78
	STD	0.12	0.11	0.10	0.11
P45	Ave ZP	24.79	24.79	24.78	24.79
	STD	0.21	0.22	0.31	0.09
P90	Ave ZP	24.80	24.79	24.82	24.80
	STD	0.17	0.17	0.22	0.10
P135	Ave ZP	24.80	24.80	24.79	24.80
	STD	0.12	0.11	0.11	0.10
	# of Stars	5,644	4,545	2,025	2,520

Table 6 shows the extracted pseudo ZP for several different GAIA G magnitude ranges. However, in this case, noise reduction was applied to these images and significantly reduced the number of stars extracted across the 40 images. This indicates there are quite a few “sources” caused by the various noise sources. For the “11-14” magnitude range, there are 5,644 stars extracted from the 40 images taken of the SA26 star field alone. The average ZP is shown for those stars along with the associated standard deviation. For the “12-14” magnitude range, 4,545 stars were used. For the “12-13” magnitude range, 2,025 stars were used. For the “13-14” magnitude range, 2,520 stars were used. Given the results in Table 6, the most accurate solution for automated relative photometry would be to noise reduce the observations and constrain the ZP calculation to the “13-14” G magnitude range.

6. POLARIZED SPECTRA OF GEO SATELLITES

After characterizing the polarization accuracy of the four channels, we collected polarized spectra of a DirecTV

cluster of geostationary satellites (DTV-10, DTV-12, and DTV-15), using the four polarization filters (P0, P45, P90, and P135). Since the USAFA-1m system employs two filter wheels in series, polarization observations can be made in combination with color filter or a diffraction grating. The observations presented here are in combination with the 200-lines-per-millimeter transmission grating to not only examine polarization as a function of wavelength, but also a function of the signal to noise ratio (SNR) given the changing counts per second across each spectrum. Fig. 6 is an example image of the DTV-10/12/15 cluster taken on 2 July 2023 UT with a 10-second exposure time and a combination of the 135° polarization filter (P135) with the grating. Because we were rate tracking the satellites, the stars appear as horizontal streaks. The satellites themselves are in the order from left to right: DTV-12, DTV-10, DTV-15. The zero-order is evident as point sources while the first-orders are the vertical streaks above their respective zero-order.

Fig 6. Image of DTV-10/12/15 taken 2 July 2023 UT with the 135° polarization filter and the 200-lines/mm transmission grating. The exposure time was 10 seconds. The horizontal lines are star streaks while the three vertical lines are the first-order diffraction patterns.

Fig. 7 is a panel of plots that show the polarized spectra for each of the polarization filters (P0, P45, P90, P135) for DTV-10/12/15. Of the three GEOs, DTV-15 had a stronger optical signal, i.e. a greater signal-to-noise ratio (SNR), which explains why the raw signal for DTV-10/12 is considerably nosier. This feature of the data from 2 July 2023 is also present in the data collected on 2 Aug 2023 as seen in Fig. 8.

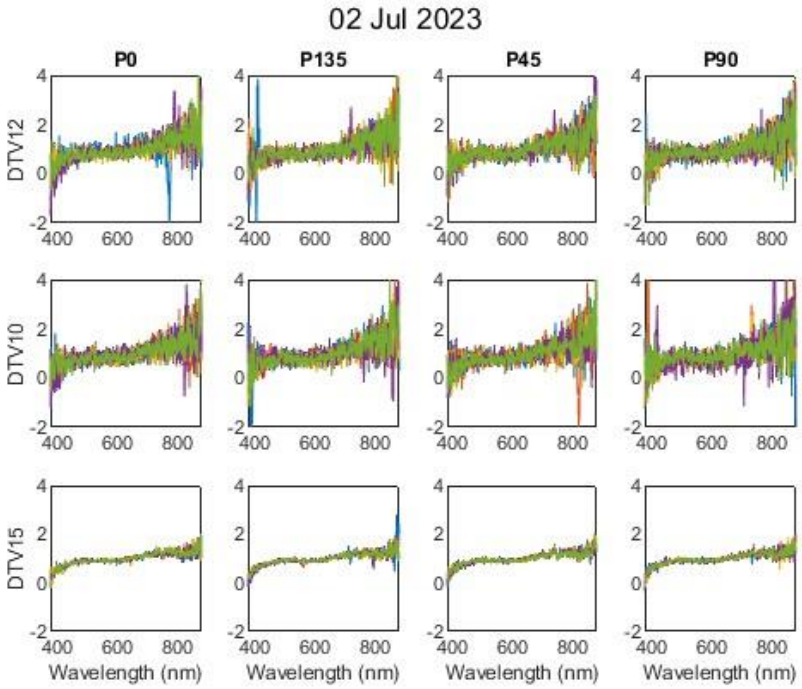

Fig. 7. Polarized spectra (normalized) of DTV-12 (top panel), DTV-10 (middle panel), and DTV-15 (bottom panel) for each of the polarization filters: P0 (first column), P135 (second column), P45 (third column), P90 (fourth column). Data collected on 2 July 2023 UT, and each plot contains data from five images. Color was arbitrarily chosen by MATLAB©.

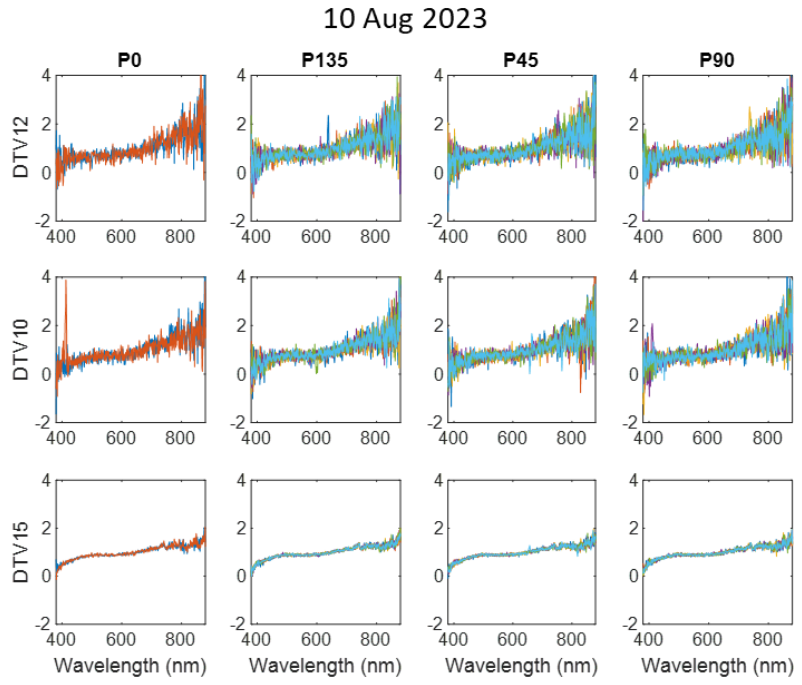

Fig. 8. Polarized spectra (normalized) of the same DTV-10/12/15 cluster taken on 2 August 2023 UT. Each plot contains data from two images. Format is the same as Fig. 7. Color was arbitrarily chosen by MATLAB©.

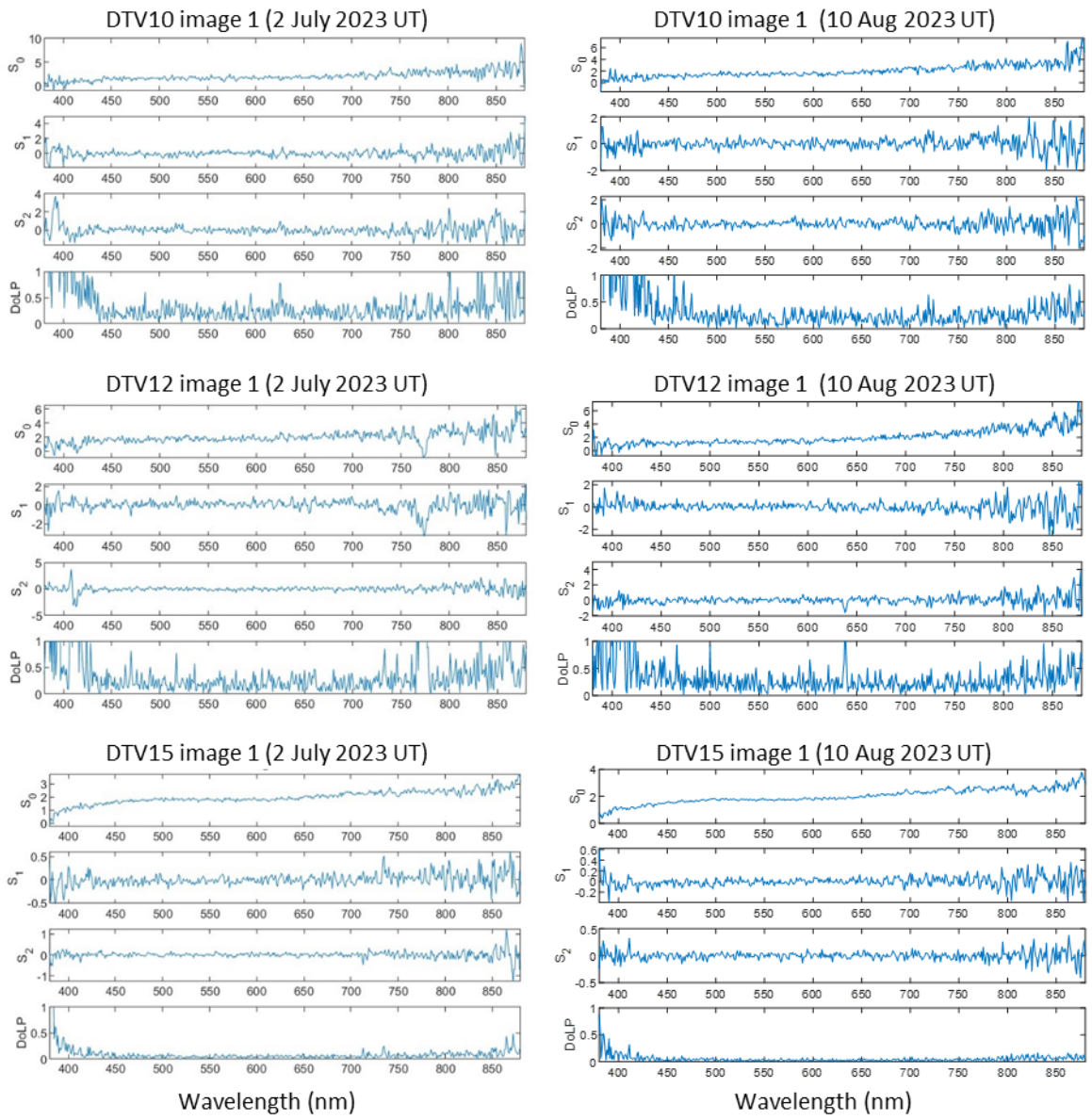

Fig. 9. Stokes parameters for DTV-10/12/15 for both nights of observations: 2 July 2023 UT (left column) and 2 August 2023 UT (right column). Each individual GEO panel consists of 4 plots: S0, S1, S2, and DOLP as a function of wavelength.

The resulting Degree-of-Linear-Polarization (DOLP) derived from the Stoke's parameters (S0, S1, S2) can been seen in Fig. 9. Due to the low signal-to-noise (SNR) of the DTV-10/12 polarized spectrum, their DOLP is highly dynamic and variable, as opposed to DTV-15's DOLP. However, even the DTV-15 DOLP shows more variability at the ends (i.e., short and long wavelengths) where the SNR is much smaller than the middle of the spectrum. Examining DTV-15's DOLP for the higher SNR portion of the spectrum appears to indicate no significant polarization.

7. CONCLUSION

We presented initial results of polarized spectra of geostationary satellites using a combination of polarization filters with a transmission grating on the USAFA-1m telescope. We described the calibration process for the polarization filters and determined that there were no statistical differences in the optical system that causes any systematic errors that need to be calibrated out. This means that future observations with the polarization filters on USAFA-1m can be processed as is without polarization correction. The initial polarized spectra of DTV-10/12/15 show that SNR plays a big role in the calculation of a GEO satellite's DOLP.

For estimation of objects of interest, relative polarization, much like relative photometry, can be used in an automated manner based on the GAIA catalog. In addition, the method is not limited to the location of known calibrated star sources. This allows one to point the telescope at a star field near an object of interest and calibrate the telescope using that field. This result makes sense due to the character of the GAIA DR2 catalog. The catalog has "G magnitudes for more than 1.69 billion sources, with precisions varying from around 1 milli-mag at the bright (G<13) end to around 20 milli-mag at G=20."[9] This allows a telescope with a large enough field of view to point anywhere and have enough stars to generate a pseudo ZP. This method also has the benefit of using relative photometry anywhere in the field and using a star field near the object of interest accounts for atmospheric extinction as well.

Future studies should 1) observe stars with known polarization characteristics to verify our calibration results, 2) quantify the effects of SNR on DOLP, 3) compare a polarized spectra to an unpolarized spectra, and 4) collect polarized spectra during the glint season.

8. ACKNOWLEDGEMENTS

We want to acknowledge the support of the Air Force Office of Scientific Research. Additionally, a portion of this paper is the result of an independent research project during the 2023 Spring semester in the Department of Physics and Meteorology at the United States Air Force Academy.

9. PUBLIC RELEASE AND DISCLAIMER

10. REFERENCES

[1] Francis K. Chun *et al* 2018 *PASP* **130** 095003
[2] Tippets, R.D., S. Wakefield, S. Young, I. Ferguson, C. Earp-Pitkins, and F.K. Chun, "Slitless spectroscopy of geosynchronous satellites," *Opt. Eng.* **54**(10), 104103 (2015). doi: 10.1117/1.OE.54.10.104103.
[3] Dunsmore, A.N., J.A. Key, R.M. Tucker, E.M. Weld, F.K. Chun, and R.D. Tippets, "Spectral Measurements of Geosynchronous Satellites During Glint Season," *J. Spacecraft and Rockets*, *Vol*. 54 *No*. 2, March 2017, pp. 349–355. doi: http://arc.aiaa.org/doi/abs/10.2514/1.A33583.
[4] Pirozzoli, M.F., L.A. Zimmerman, M. Korta, A.D. Scheppe, F.K. Chun, M.K. Plummer, C.N. Harris, D.M. Strong, "Calibration, Sensitivity Analysis, and Demonstration of a Basic Polarimeter for Artificial Satellite Observations," *Adv. Space Res.*, pp. 581-591, 2022.
[5] Albrecht, E.M., A. M. Jensen, E.G. Jensen, K.A. Wilson, M.K. Plummer, J.A. Key, D.S. O'Keefe, F.K. Chun, D.M. Strong, C.P. Schuetz-Christy, "Near-Simultaneous Observations of a Geosynchronous Satellite Using Two Telescopes and Multiple Optical Filters," *J Astronaut Sci* (2022). https://doi.org/10.1007/s40295-021-00292-x
[6] Wetterer, C.J., D.M. Strong, T.W. Giblin, and F. Chun, "Spectral Calibrations of the USAFA 1-Meter for GEO Satellite Spectral Signatures," *The 2023 AMOS Technical Conference Proceedings*, The Maui Economic Development Board, Inc., Kihei, Maui, HI, (2023)
[7] Busso, G., C. Cacciari, J.M. Carrasco, F. De Angeli, D.W. Evans, C. Fabricius, C. Jordi, P. Montegriffo, E. Pancino, "Gaia DR2 documentation Chapter 5: Photometry", gdr2.rept, 2018. https://gea.esac.esa.int/archive/documentation/GDR2/
[8] Bertin, Éric and Stéphane Arnouts. "SExtractor: Software for source extraction," *Astronomy & Astrophysics Supplement Series* 117 (1996): 393-404.
[9] Gaia DR2 contents - Gaia - Cosmos (esa.int) https://www.cosmos.esa.int/web/gaia/dr2